Title:

Synaptic mechanisms that contribute to spatial tuning in primary auditory cortex.

Abbreviated title:

Synaptic mechanisms shaping A1 spatial tuning.

Authors:

Alfonso junior Apicella[1,2,†], Mohammad Dastjerdi[1,2,‡], and Michael Robert DeWeese[1,2,3]

1 Helen Wills Neuroscience Institute, University of California, Berkeley, CA

2 Redwood Center for Theoretical Neuroscience, University of California, Berkeley, CA

3 Department of Physics, University of California, Berkeley, CA

† Current address: Feinberg School of Medicine, Northwestern University, Chicago, IL

‡ Current address: Department of Neurology and Neurological Sciences, Stanford University School of Medicine, Palo Alto, CA

E-mail: deweese@berkeley.edu, mdast2u@gmail.com, a-apicella@northwestern.edu

Corresponding Author:

Michael R. DeWeese, deweese@berkeley.edu

Number of Pages: 41 (not including figures)
Number of Figures: 6 figures; no tables
Number of words – Abstract: 227
Number of words – Introduction: 500
Number of words – Discussion: 1514

Keywords: auditory, cortex, whole-cell recording, rat, neural coding, spatial hearing, localization, intracellular recording, A1, primary auditory cortex,

Acknowledgements:

This work was supported by grants from the Hellman Family Faculty Fund and the McKnight Foundation, as well as a NARSAD Young Investigator Award to A.j.A.

Synaptic mechanisms that contribute to spatial tuning in primary auditory cortex.

Alfonso junior Apicella[1,2,†], Mohammad Dastjerdi[1,2,‡], and Michael Robert DeWeese[1,2,3,*]

1 Helen Wills Neuroscience Institute, University of California, Berkeley, CA

2 Redwood Center for Theoretical Neuroscience, University of California, Berkeley, CA

3 Department of Physics, University of California, Berkeley, CA

† Current address: Feinberg School of Medicine, Northwestern University, Chicago, IL

‡ Current address: Department of Neurology and Neurological Sciences, Stanford University School of Medicine, Palo Alto, CA

* To whom correspondence should be addressed; deweese@berkeley.edu

Abstract

Neurons in primary auditory cortex (A1) tend to respond more strongly to sound sources located contralateral to the recorded neuron compared to ipsilateral sources, but the synaptic mechanisms underlying this asymmetry are largely unknown. We have used *in vivo*, whole-cell patch clamp methods to directly measure the timecourses of excitatory and inhibitory synaptic drive to individual A1 neurons in anesthetized rats in response to free-field acoustic stimulation from ipsilateral and contralateral sound sources. We find that both excitatory and inhibitory synaptic conductances tend to exhibit greater peak values and shorter latencies in response to contralateral sources compared to responses to ipsilateral sources. We also observe steeper rising phases of the excitatory conductance changes in response to contralateral sounds, but no significant difference for inhibitory conductance changes. Moreover, in response to free-field acoustic stimulation from a given location, the relative magnitudes of excitation and inhibition are approximately sound intensity-invariant, though the ratio of excitatory and inhibitory input can depend somewhat on sound source location. Our results are broadly

consistent with the simple model that both contralateral and ipsilateral sound sources typically elicit stereotyped synaptic responses with inhibition following excitation by a short delay and an approximately fixed ratio of peak excitatory and inhibitory amplitudes, such that the responsiveness of the neuron to different sound intensities and locations is governed by the overall scaling of the total peak conductance.

Introduction

A longstanding goal in auditory research is to uncover the mechanisms underlying auditory-evoked spiking activity in primary auditory cortex (A1). Understanding the role played by synaptic inhibition is central to this goal. In particular, because the thalamocortical projection is purely excitatory, inhibitory input to A1 neurons necessarily involves a cortical component. Intriguingly, excitation and inhibition typically exhibit nearly identical spectral tuning in A1 (Wehr and Zador, 2003; Zhang et al., 2003; Tan et al., 2004; Wu et al., 2006; Wu et al., 2008) in response to sounds originating from sources contralateral to the recorded neuron, but it is not known what role cortical inhibition might play in shaping spatial sensitivity of A1 neurons.

Primarily through lesion studies, it is known that A1 is necessary for sound source localization, particularly along the horizontal plane ((Sanchez-Longo and Forster, 1958; Klingon and Bontecou, 1966; Heffner and Masterton, 1975; Jenkins and Masterton, 1982; Jenkins and Merzenich, 1984; Kavanagh and Kelly, 1987; Talwar et al., 2001; Nodal et al., 2010); *c.f.* (Kelly, 1980)). Consistent with this, neurons in A1 often exhibit preferences for some patterns of binaural stimulation over others (King et al., 2007). Specifically, most A1 neurons respond preferentially to sounds originating from sources

contralateral to the neuron, and to dichotic stimulation that is louder at the contralateral ear. Response strength for neurons with a preference for lateralized stimulation is typically monotonic in azimuth (Middlebrooks and Pettigrew, 1981; Werner-Reiss and Groh, 2008; Bizley et al., 2009), though some neurons are tuned to intermediate values (Middlebrooks and Pettigrew, 1981; Schnupp et al., 2001). One study of subthreshold responses (Chadderton et al., 2009) found shorter latencies for post-synaptic potentials (PSPs) in response to contralateral sounds, and larger peak amplitudes for preferred locations, but this left open the question of whether this reflected changes in excitatory or inhibitory synaptic drive or some combination.

Most neurons in the ventral division of the medial geniculate body of the auditory thalamus (MGBv; the major thalamic source of excitatory input to A1) also exhibit a preference for contralateral stimulation (Clarey et al., 1995). This led us to wonder whether spatial sensitivity in A1 might be inherited from thalamocortical projections in a straightforward way. Using *in vivo* whole-cell patch clamp methods (DeWeese and Zador, 2004, 2006; DeWeese, 2007), we have recorded post-synaptic currents at multiple holding potentials in A1 of the anesthetized rat, allowing us to directly measure the timecourses of excitatory and inhibitory synaptic conductances of individual neurons (Borg-Graham et al., 1998; Hirsch et al., 1998; Anderson et al., 2000; Wehr and Zador, 2003; Wu et al., 2008; Sun and Dan, 2009; Dorrn et al., 2010) in response to white-noise bursts originating from either side of the subject's head.

We find that both excitation and inhibition exhibit greater peak values and shorter latencies in response to contralateral sources. Relative latencies and magnitudes of excitation and inhibition are roughly invariant to stimulus intensity and sound source

location, suggesting that the magnitude of the total conductance change largely dictates spatial sensitivity in A1.

Materials and Methods

Surgery

All experimental procedures were performed in accordance with National Institutes of Health guidelines and approved by the Animal Care and Use Committee at University of California, Berkeley. We followed a surgical procedure similar to those described in detail elsewhere (DeWeese et al., 2003; DeWeese and Zador, 2004, 2006; DeWeese, 2007). Adult (postnatal day 40-60), male, Long-Evans rats were first anesthetized with ketamine (90 mg/kg) and xylazine (10 mg/kg). After the animal was deeply anesthetized, it was placed in a custom naso-orbital restraint that left the ears free and clear. Lidocaine was applied to the muscles and skin of surgical areas prior to incisions. A cisternal drain was performed. After removing a section of temporomandibular muscle, a small craniotomy (maximum size of 1.0 mm × 1.0 mm) and durotomy were performed over the left (primary) auditory cortex. The position of the craniotomy was determined by its distance from bregma (4.5 mm posterior and 4 mm lateral), and its relationship to other bone sutures. The presence of clear auditory local field potentials was further used as physiological criteria to confirm the location of the auditory cortex. Based on the anatomical landmarks and physiological features of the recorded sound-evoked response we expect that the neurons recorded in this study were in the primary auditory cortex.

Prior to the introduction of electrodes, the cortex was covered with physiological buffer (in mM: NaCl, 127; Na_2CO3, 25; NaH_2PO_4, 1.25; KCl, 2.5; $MgCl_2$, 1; glucose, 25) mixed with 1.5% agar. Body temperature was monitored rectally and maintained at 35°C – 37°C using a feedback controlled blanket (Harvard Apparatus). Breathing and response to noxious stimuli were monitored throughout the experiment, and respiration was monitored with a chest-mounted piezoelectric strap; supplemental doses of ketamine were provided as needed based on these indicators.

Sound Stimuli

All experiments were conducted in a double-walled sound booth (Industrial Acoustics Company). Binaural free-field stimuli were presented using a computer (custom built PC running Microsoft Windows XP) connected to an amplifier (Tucker Davis Technologies), which drove two calibrated speakers (Super Tweeter, Radio Shack) located 7.5 cm lateral to, and facing, the ipsilateral (left) and contralateral (right) ears, respectively. Calibration was performed with a microphone (Brüel & Kjaer 4138 microphone with 2670 preamplifier) positioned at the location of the ear that would have been facing the speaker being calibrated had the rat been present. Our stimuli consisted of 100 ms duration, band-pass (2kHz to 50kHz) white-noise bursts presented in a random sequence from a range of 30 to 90 dB SPL with increments of 10 dB SPL. Each unique stimulus was presented 10 times from each of the two speakers, for a total of 10x7x2 = 140 stimulus presentations per full cycle. Onsets and terminations of each noise burst followed an envelope described by 3 msec 0% – 100% cosine-squared ramps. Each of the seven intensities was presented from each speaker one time in

each of the 10 consecutive blocks of 14 stimuli, and each block followed a different pseudorandom sequence.

Stimulus delivery and data acquisition were achieved by two computers, a “master” computer (a custom built PC running Microsoft Windows) that controlled a “slave” computer (a custom built PC running Linux) that performed real-time control. The master computer ran a data acquisition program that was a slightly modified version of *ExperSolo*, a computer program written in the Matlab programming language by Tomáš Hromádka, which built on earlier software written by Anthony Zador, Zachary Mainen, and Carlos Brody. The slave computer performed real-time control of the stimulus delivery using a computer program written by Calin Culianu in the C++ programming language.

Electrophysiology

Following methods described in detail elsewhere (DeWeese et al., 2003; DeWeese and Zador, 2004, 2006; DeWeese, 2007), we used standard *in vivo* blind whole-cell patch clamp recording methods (Ferster and Jagadeesh, 1992; Metherate and Ashe, 1993; Nelson et al., 1994; Hirsch et al., 1995; Covey et al., 1996; Gray and McCormick, 1996; Azouz et al., 1997; Moore and Nelson, 1998; Bringuier et al., 1999; Zhu and Connors, 1999a, b; Freeman et al., 2002; Margrie et al., 2002; Cang and Isaacson, 2003; Wehr and Zador, 2003; Zhang et al., 2003; Bureau et al., 2004; Manns et al., 2004; Tan et al., 2004; Zhu and Zhu, 2004; Las et al., 2005; Wehr and Zador, 2005; Meliza and Dan, 2006; Wu et al., 2006; Froemke et al., 2007; Liu et al., 2007; Tan et al., 2007;

Houweling and Brecht, 2008; Okun and Lampl, 2008; Priebe, 2008; Scholl et al., 2008; Scholl and Wehr, 2008; Wu et al., 2008; Gao et al., 2009).

Whole-cell recordings were performed using a 200B Axopatch amplifier (Axon Instruments), using patch pipettes (3–5 MΩ) filled with (in mM) 130 cesium gluconate, 5 NaCl, 10 HEPES, 0.2 EGTA, 12 phosphocreatine, 3 Mg-ATP, and 0.2 Na-GTP, 2 QX-314, (7.25 pH; 290–300 mOsm). Series resistance for whole-cell recording was ≤50 MΩ and continuously monitored. Cells in which series resistance changed by >10% were excluded. Cells from layer 1 to layer 6 were targeted based on the z-axis readout of an MP-285 micromanipulator (Sutter). The search for neurons was conducted solely based on pipette's resistance and not on spiking activity. LFPs were recorded using either a patch pipette (0.5–1 MΩ) filled with NaCl 1 M or a tungsten electrode (FHC) positioned in layer 2/3 ~ 0.5-0.8 mm anterior to the patch electrode recording site.

30 neurons (from 16 animals) passed our criteria for inclusion in our analysis: we required that at least two stable recordings were obtained at different holding potentials, each lasting at least as long as one half cycle of the stimulus protocol, which included 5 presentations of each of the unique stimuli (*i.e.*, stimuli with unique speaker–intensity pairs). In addition, resting potentials had to be below -50 mV (uncorrected for liquid junction potential); the range of uncorrected membrane potential readings for the neurons included in our analysis was -77 mV ≤ V_m ≤ -54 mV. For our internal solution and recording conditions, we estimate that the liquid junction potential was approximately -10 mV for our recordings.

Measuring timecourses of excitatory and inhibitory conductances with whole-cell patch clamp recording

To measure the timecourses of both excitatory and inhibitory conductances of individual A1 neurons in intact animals, we must 1) have access to the subthreshold activity inside the neuron, 2) prevent nonlinearities such as voltage gated channels in the cell membrane from obscuring the underlying conductance changes, and 3) obtain at least two independent measurements of electrical activity inside the neuron at every time point. *In vivo* whole-cell recording in voltage-clamp mode satisfies all three of these requirements and has been used successfully to measure synaptic conductances, first in visual cortex (Borg-Graham et al., 1998) and more recently in auditory cortex (Wehr and Zador, 2003; Zhang et al., 2003; Tan et al., 2004; Wehr and Zador, 2005; Wu et al., 2006; Liu et al., 2007; Wu et al., 2008) (see also (Hirsch et al., 1998; Anderson et al., 2000; Ojima and Murakami, 2002; Las et al., 2005)). Much of this section follows the discussion in the Supplementary Information for (Wehr and Zador, 2003).

The basic analysis is as follows. Under voltage clamp conditions, the total current recorded at the soma is:

$$I_s(t) = g_e(t)\,(V_h - E_e) + g_i(t)\,(V_h - E_i) + g_{IN}\,(V_h - E_{rest}), \qquad (1)$$

where $I_s(t)$ is the current measured at the soma at time t (measured with respect to stimulus onset) under voltage clamp at the holding potential V_h; $g_e(t)$ and $g_i(t)$ are, respectively, the time-varying excitatory and inhibitory synaptic conductance changes triggered by the stimulus; E_e and E_i are, respectively, the corresponding synaptic driving forces; and g_{IN} and E_{rest} are the input conductance and resting potential in the absence

of stimulus-locked synaptic input. In a typical experiment, the excitatory and inhibitory driving forces are given by the Nernst equation, (E_e = 0 mV and E_i = –85 mV, both uncorrected for junction potential, under our conditions); the holding potential V_h is under our control; the resting input conductance g_{IN} and the resting membrane potential E_{rest} are measured using voltage steps delivered during silent periods, and the time-varying current $I(t)$ is measured continuously. This equation assumes an isopotential neuron, and thus neglects the effect of dendritic structure, and it neglects nonlinear (voltage-dependent) conductances as well. The effect of such nonlinearities can be minimized by recording under electrical or pharmacological conditions that block many of these conductances.

Eq. (1) has two unknowns, $g_e(t)$ and $g_i(t)$, at each point in time, which we can estimate by making separate measurements, $I_1(t)$ and $I_2(t)$, under two different holding potentials V_1 and V_2, and then solving for $g_e(t)$ and $g_i(t)$ in the pair of coupled equations resulting from plugging these quantities into Eq. (1). Thus, any pair of current measurements obtained at two different holding potentials generates an estimate for the contributions of the excitatory and inhibitory conductance changes. In practice, we perform linear regression on the data points we have for the set of unique holding potentials to estimate the slope G_o and intercept I_o of the idealized linear fit to the current-voltage relation (Fig. 2B),

$$I_s(t) = G_o(t)\ V_s - I_o(t), \qquad (2)$$

where $I_s(t)$ is the observed current at time t; V_s is the holding potential at the soma; $G_o(t)$ is the best fit of the total conductance at each point in time, representing the sum of the

actual underlying conductances, $G_o(t) = g_e(t) + g_i(t) + g_{IN}$; and $I_o(t)$ is the best fit value at the intercept of the current-axis, representing the weighted sum of the actual reversal potentials, $I_o(t) = g_e(t)\, E_e + g_i(t)\, E_i + g_{IN}\, E_{rest}$.

The analysis outlined in Eqs. (1,2) yields the exact timecourse for the underlying excitatory and inhibitory conductance changes only under ideal conditions, when all the assumptions of the derivation are met. Generally, the assumptions behind Eq. (1) will not be met exactly (which is also generally the case for *in vitro* recordings), so the estimated conductance changes might be inaccurate.

The two most significant sources of error are voltage-dependent conductances (Reyes, 2001), and escape from subsynaptic voltage clamp due to cable attenuation (so-called "space-clamp" artifacts (Brown et al., 1992; Claiborne et al., 1992; Spruston et al., 1993; Zador et al., 1995; Mainen et al., 1996; Williams and Mitchell, 2008)). We used a Cs-based internal solution and the lidocaine derivative QX-314 in our recording pipette to minimize the first source of error, but even when voltage-dependent effects cannot be prevented, they can still be detected as a deviation from linearity of the synaptic I-V relation (Eq. (2); Fig. 2B). Linearity of the synaptic I-V relation provides an internal control for voltage-gated conductances but not for attenuation and saturation effects, but one can estimate the sign and magnitude of typical errors. However, in the absence of voltage-dependent conductances, the synaptic current recorded under voltage clamp is still a linear function of somatic holding potential even when there is imperfect control of the subsynaptic membrane. By contrast, the recorded current is a sublinear function of synaptic conductance, due to the well-known saturation effect arising from decreased driving force — as current enters the dendrite, the membrane potential close to the

synapse is momentarily pushed towards the reversal potential of the particular species of ion comprising the current. Thus, the linearity of the synaptic *I-V* relation provides an internal control for voltage-gated conductances but not for attenuation and saturation effects.

Space-clamp artifacts cannot always be avoided, but we can estimate the sign and magnitude of typical errors. Consider a synaptic conductance change $g_e(t)$ at the dendritic location of the excitatory synapse, and the resulting somatic $I_s(t)$ recorded at the soma while clamping the soma to V_s. The potential change at the dendrite is only a fraction of the voltage difference between rest and the somatic holding potential, so the steady state voltage at the synapse, V_e, prior to synaptic activation, is $V_e = A\ V_s$, where we have defined the voltage attenuation factor $0 \le A \le 1$, which is a constant determined by the electrotonic structure of the neuron. For synapses on the soma $A = 1$, whereas A can be much smaller for a distal synapse on a "leaky" dendrite. If we neglect saturation effects, it can be shown (Koch et al., 1982; Zador et al., 1995) that

$$I_s = (G_e\ A^2)\ V_s - A\ E_e\ G_e, \qquad (3)$$

which relates the measured somatic current I_s to the (unknown) electrotonic structure of the neuron. Comparison with Eq. (2) shows that G_e is underestimated by a factor A^2 — one factor of A comes from the loss of current as it travels from the synapse to the soma, and the other factor of A reflects our inability to perfectly clamp the subsynaptic membrane to our desired holding potential. Estimates of A for cortical neurons (Zador et al., 1995) based on morphology indicate that A is typically above 0.7, and can be as high as 0.95 for proximal synapses, indicating that under these conditions G_e will be

underestimated by a factor of (0.7^{-2}) at most, so in the absence of saturation effects our estimate is within a factor of two of the correct value.

Moreover, since our ultimate goal is to understand how synaptic input shapes the spiking response of the neuron, only one of those two factors of *A* represents a true "error" for our purposes — namely, the factor arising from our inability to clamp the subsynaptic membrane to our desired steady-state holding potential. In fact, even the saturation effects we neglected in our calculation are best left ignored since they, too, represent a true inability of electrotonically distant synapses to affect spike production in or near the soma.

Eq. (3) shows that, like G_s, E_s is also in error. A more detailed analysis ((Spruston et al., 1993); see also Supplementary Information for (Wehr and Zador, 2003)) shows that the error in our estimate of the neuron's reversal potential results in a bias in the decomposition into excitatory and inhibitory conductances, such that we will overestimate the relative contribution from excitatory synapses for roughly balanced levels of excitation and inhibition. However if inhibitory synapses are more proximally distributed than excitatory synapses, as is typical for many cortical neurons, this will cause us to underestimate the excitatory contribution more than the inhibitory input due to differences in the voltage attenuation factor *A* discussed above. Fortunately, these sources of error would tend to counteract one another given reasonable assumptions about neuronal morphology and synaptic distribution.

The preceding analysis implies that most errors in our conductance measurements will be underestimates, and that the magnitude of our errors will likely be under 30% in most

cases, though it is worth noting that some empirical measurements of measured current at the soma in response to injected current at a range of locations in the dendrites have demonstrated larger errors in estimated conductance changes (Williams and Mitchell, 2008). More importantly, although we cannot be confident about the absolute magnitude of synaptic conductance changes, we have designed our experiments to rely only on the *relative differences* between these changes as stimulus parameters are varied.

Finally, we will point out that some of our analyses depend on the relative timing of the onset of the excitatory and inhibitory synaptic input, rather than the amplitude of the conductance changes. Fortunately, the *timing* of abrupt changes in either the excitatory or inhibitory synaptic conductance is less susceptible to errors described above than measurements of the absolute amplitude.

Peak and latency analyses

We defined the peak (excitatory or inhibitory) conductance as the maximum value of the trial-averaged conductance timecourse in a 60 msec window following the stimulus onset, minus the average conductance during the 50 msec preceding stimulus onset. We determined the latency of the onset of the stimulus-evoked conductance change by first fitting a straight line to the two points on the rising conductance that reached 10% and 90% of the peak value relative to the baseline conductance level. We defined the onset latency of the conductance change as the delay from stimulus onset to the point where the linear fit to the rising conductance crossed the baseline value. Peak and latency values were not included in our analysis for conductance timecourses that did not achieve a peak within 60 msec following stimulus onset (e.g., if the conductance

decreased during this time period relative to pre-stimulus baseline, or if the conductance rose monotonically so that the maximum value for the entire interval was achieved at the termination of the 60 msec time window). Group comparisons were made using the two-tailed Wilcoxon signed rank test, unless otherwise noted. Significance was set at $p < 0.05$.

Results

Measuring timecourses of excitatory and inhibitory synaptic conductances

Our goal is to determine the mechanisms underlying spatial selectivity in A1. Even at the level of spiking responses, binaural responses cannot be reliably inferred from measurements of monaural responses alone (Zhang et al., 2004). Moreover, it is worth making explicit that binaural extracellular spiking records alone cannot determine which of the possible synaptic input patterns is responsible for an observed change in responsiveness. Fig. 1 illustrates this point with simple cartoons of several candidate mechanisms underlying differences in firing probability. The hypothetical neuron represented in the figure responds with high probability to contralateral sounds (Fig. 1A, *right*) but infrequently to ipsilateral sounds (Fig. 1A, *left*), as is typical for A1 neurons. Four candidate mechanisms that could each underlie this stimulus preference are illustrated: a difference in the amplitude of excitation alone (Fig. 1B); a difference in the amplitude of inhibition alone (Fig. 1C); comodulation of the amplitudes of excitatory and inhibitory synaptic inputs (Fig. 1D); and a difference in the relative timing of the onsets of excitation and inhibition with no change in the amplitudes of either excitation or inhibition (Fig. 1E). Of course, there are many other possibilities, such as combinations of these specific mechanisms. Thus, many patterns of synaptic input to the neuron can

give rise to the same stimulus preference as measured at the level of the spiking output of the neuron.

In order to measure the timecourses of synaptic excitatory and inhibitory drive to A1 neurons in the intact animal, we used *in vivo* whole-cell patch clamp methods (DeWeese and Zador, 2004, 2006; DeWeese, 2007) to recorded postsynaptic currents in voltage-clamp mode (see Materials and Methods). Fig. 2A shows three current traces from an *in vivo* whole-cell voltage clamp recording of an A1 neuron. Each trace is an average of 250 trials during which the same white noise burst was presented. Each of the three traces corresponds to a different holding potential of the electrode, and the current that is plotted is the amount needed to maintain this potential throughout the trial. Fig. 2B demonstrates the near perfect linearity of the current-voltage relation for this recording, indicating that nonlinearities in the neuron, such as voltage-gated channels not sufficiently blocked by QX-314 or Cesium ions, did not distort our measurement of the timecourse of synaptic input (see Materials and Methods). Fig. 2C presents the resulting estimates for the full timecourse of total conductance (*black line*; g_{syn}) and the individual excitatory (*green*; g_e) and inhibitory (*red*; g_i) conductances obtained using the procedure outlined above. Note that both excitation and inhibition start off flat and then rise abruptly at a latency of just under 20 msec following the onset of the stimulus (*blue line*), before decaying back down to their original steady state values.

Peak conductance is greater in response to contralateral sound sources for both excitation and inhibition

The example neuron shown in Fig. 3 exhibited a pattern of excitatory and inhibitory synaptic conductance changes that was in broad agreement with the cartoon shown in Fig. 1D: both the excitatory and inhibitory drive to the neuron tended to be larger in response to contralateral sound sources for most stimulus intensities tested.

This was in fact the case across our population of recorded neurons. The scatter plot in Fig. 4A exhibits a clear trend for both excitatory and inhibitory conductances — in each case, peak conductance values were typically larger in response to contralateral sounds compared to ipsilateral sounds of the same intensity (excitation: $p = 2.1\times10^{-8}$; inhibition: $p = 1.7\times10^{-12}$; all p values reported here are for the two-tailed Wilcoxon signed rank test.). This trend was also evident across the population when we restricted our analysis to responses to the loudest sounds we tested (Fig. 4B; excitation: $p = 2.3\times10^{-4}$; inhibition: $p = 0.0098$). Thus, across the population, both synaptic excitation and inhibition to individual A1 neurons exhibited the same contralateral preference as typical spiking responses in A1 and in the ventral division of the medial geniculate body (MGBv), the major thalamic source of excitatory input to A1 (the “lemniscal pathway” (Hu et al., 1994)).

Onset latencies are shorter in response to contralateral sound sources for both excitation and inhibition

As one might expect given the stronger excitatory and inhibitory drive from contralateral sound sources described above, we found that both excitatory and inhibitory onset latencies were typically shorter in response to contralateral sounds compared to ipsilateral sounds (Fig. 4C; excitation: $p = 5.2\times10^{-4}$; inhibition: $p = 1.1\times10^{-6}$). This trend

was also evident for responses restricted to the loudest sound level tested (Fig. 4D; excitation: $p = 0.0010$; inhibition: $p = 9.3\times10^{-5}$).

Excitation and inhibition are approximately balanced for individual neurons in response to sounds from specific locations

Excitation and inhibition are approximately balanced for individual A1 neurons, so that the ratio of peak excitatory and inhibitory conductances is roughly constant across sound intensity levels for specific sound locations. Fig. 5A presents a scatter plot for an example neuron exhibiting a strong correlation between peak excitatory and inhibitory conductances across sound intensity levels for a contralateral sound source ($r = 0.81$, Pearson product-moment correlation coefficient), as well as for an ipsilateral sound source ($r = 0.87$). For this neuron, the ratio of the peak values of inhibitory to excitatory conductance was different for contralateral sounds (~2.5) and ipsilateral sounds (~1.1) by more than a factor of two, but the correlation across intensities for either location was high.

The strong correlation between peak values of excitation and inhibition in response to sounds of different intensity originating from the same location was evident across the population. Peak excitatory and inhibitory conductances of many neurons were strongly correlated, with population averaged correlations of $r = 0.74 \pm 0.05$ and 0.54 ± 0.09 (mean ± SEM) for contralateral and ipsilateral sources, respectively (Fig. 5B). Note that correlation coefficients for about half of the neurons are clustered near $r = 1$ for both ispilateral and contralateral sound source locations. Fig. 5C presents a scatterplot of peak excitatory and inhibitory conductances for all 30 neurons and all sound intensity levels, illustrating the clear correlation amongst the aggregate responses across all

neurons and conditions (all contralateral responses: r = 0.64; all ipsilateral responses: r = 0.49; all responses: r = 0.54). Thus, while some neurons exhibited different ratios of excitatory to inhibitory peak values for sounds originating contralateral or ipsilateral to the recorded neuron (*e.g.*, Fig. 5A), this ratio was roughly consistent across the population for all stimulus intensities and both locations.

In keeping with the clear correlation between peak excitatory and inhibitory drive, we found that the fraction of excitatory conductance — $g_{ep}/(g_{ep} + g_{ip})$, where g_{ep} (g_{ip}) is the peak excitatory (inhibitory) conductance — was peaked near the intermediate value of 0.35 for both contralateral and ipsilateral sources, which was also close to the mean values for each distribution (contralateral: μ ± SEM = 0.39 ± 0.01; ipsilateral: μ ± SEM = 0.44 ± 0.01).

Excitation precedes inhibition for both ipsilateral and contralateral sounds

As illustrated by the histogram shown in Fig. 5E, excitation tended to arrive slightly sooner than inhibition for both contralateral ($t_i - t_e$ = 0.73 msec, p = 0.042) and ipsilateral ($t_i - t_e$ = 1.3 msec, p = 0.0035) sound sources, as previously reported for synaptic responses to contralateral sounds in response to pure tones (Wehr and Zador, 2003; Zhang et al., 2003; Tan et al., 2004; Wu et al., 2006; Wu et al., 2008).

The slope of the initial rising phase of synaptic excitation is greater in response to contralateral sounds than for ipsilateral sounds

Chadderton and colleagues (Chadderton et al., 2009) reported that rising slopes of post-synaptic potentials (PSPs) were greater in response to contralateral sounds

compared with responses from ipsilateral sounds, which led us to wonder whether this reflected changes in the initial rising phase of synaptic excitation, inhibition, or both.

As shown in Fig. 6A, the initial rising phase of the excitatory conductance change elicited by contralateral sounds was steeper than that elicited by ipsilateral sounds ($p = 4.5\times10^{-4}$). However, we did not find a significant difference in slope of the initial rising phases of inhibitory synaptic responses to contralateral vs. ipsilateral sounds ($p = 0.27$). Our data indicate that the spatial dependence of the slope of the rising phase of PSPs in A1 result from differences in the excitatory synaptic drive alone.

Finally, we observed (Fig. 6B) that inhibitory conductances had steeper rising phases than excitatory conductances for both contralateral ($p = 1.5\times10^{-5}$) and ipsilateral ($p = 1.2\times10^{-5}$) sound sources.

Discussion

We have used *in vivo* whole-cell patch clamp recording in voltage clamp mode to measure the timecourses of excitatory and inhibitory synaptic conductances in individual A1 neurons in response to free-field acoustic stimulation consisting of brief white noise bursts originating from either side of the subject's head.

Our data are broadly consistent with the cartoon shown in Fig. 1D — for both the excitatory and inhibitory synaptic drive to A1 neurons, amplitudes tend to be higher (Fig. 4A,B) and latencies tend to be shorter (Fig. 4C,D) in response to contralateral sounds compared to ipsilateral sounds, suggesting that contralateral-preferring presynaptic population(s) drove both excitation and inhibition to the recorded neurons. Excitation

and inhibition were approximately balanced (Fig. 5A-D), and latencies were systematically greater for inhibitory responses compared with excitation (Fig. 5E), consistent with the simple model that synaptic responses to sounds originating from a particular location are approximately stereotyped, such that the scale of the overall conductance change largely determines the responsiveness of the neuron, as has been found for frequency tuning to contralateral sounds (Wehr and Zador, 2003; Zhang et al., 2003; Tan et al., 2004; Wu et al., 2006; Wu et al., 2008). We find that the slope of the rising phase of excitatory synaptic drive to A1 neurons is greater for contralateral sounds, whereas inhibition is not significantly modulated by sound source location. Finally, we find that the onset of inhibition is steeper than that of excitation, for both ipsilateral and contralateral sound sources.

The circuit mechanisms underlying sound source localization are important — sound direction cues provide useful information for associating the sounds we hear with the people, animals or objects that produce them. While most sensory modalities have a spatial component, spatial coding in audition is unlike vision or somatosensation — modalities for which some spatial dimensions are represented in the periphery by an ordered array of sensory neurons. Instead, acoustic signals carry information about sound source location through binaural cues, such as the relative intensity (interaural level difference, ILD) and timing (interaural time difference, ITD) of the sound pressure level at the two ears (King et al., 2001; McAlpine, 2005). Moreover, the head, external ears, and upper body act as spectral filters, resulting in the attenuation of certain frequencies in a direction dependent manner (Schnupp et al., 2003). As a result, the interplay between spectral filtering and sound source location can be exploited by the

auditory cortex (AC) in order to localize and isolate desired sounds from a background of distractors.

In this study we have divided the synaptic drive to individual neurons into separate contributions from excitatory and inhibitory presynaptic inputs. Of all presynaptic subpopulations we might isolate, inhibitory inputs are perhaps the most informative. The thalamocortical projection is purely excitatory, so inhibitory input to A1 neurons necessarily involves a cortical component. Moreover, inhibition can play surprising roles in spatial tuning, as it does in the inferior colliculus (Sanes et al., 1998).

Previous studies have probed the binaural spiking responses of A1 neurons using both dichotic presentation of simple test stimuli (Hall and Goldstein, 1968; Brugge et al., 1969; Imig and Adrian, 1977; Kelly and Sally, 1988; Brugge et al., 1994; Brugge et al., 1996; Irvine et al., 1996; Rutkowski et al., 2000b; Mrsic-Flogel et al., 2001; Zhang et al., 2004; Mrsic-Flogel et al., 2005; Campbell et al., 2006) and varying sound source location during free field stimulation (Middlebrooks and Pettigrew, 1981; Imig et al., 1990; Rajan et al., 1990; Stecker et al., 2005; Bizley et al., 2009). Many investigators have relied on such spiking responses in A1 to infer the presence of inhibition (*e.g.*, (Suga, 1971; Voigt and Young, 1980; Phillips and Cynader, 1985; Calford and Semple, 1995)). In fact, following a scheme devised for the superior olive (Goldberg and Brown, 1969), A1 neurons have often been classified in terms that evoke the putative synaptic inputs presumed to underlie the observed spiking responses (Zhang et al., 2004): neurons that respond to monaural stimulation to either ear are labeled “EE,” where E refers to the “excitatory” effect of the stimulation, and neurons that respond to monaural stimulation only from the contralateral (ipsilateral) ear are labeled “E0” (“0E”). Units

whose responses are suppressed by simultaneous stimulation to both ears compared to stimulation of the "excitatory" ear alone has been termed an "inhibitory" binaural interaction, designated EE/I, E0/I, or 0E/I.

Despite the longstanding interest in cortical mechanisms of spatial hearing, we are only aware of one published study (Ojima & Murakami, 2002) attempting a direct measurement of excitatory and inhibitory synaptic drive to individual cortical neurons for varying sound source locations or dichotic stimulation conditions. Similar to the many attempts to infer the presence of inhibition from the suppression of spiking, Ojima and Murakami inferred inhibitory input to A1 neurons by identifying epochs of hyperpolarization in post-synaptic potentials (PSPs) using in vivo whole-cell recording in current clamp mode.

Using similar current-clamp recording methods, Chadderton and colleagues (Chadderton et al., 2009) found that PSPs in A1 neurons tend to have steeper initial rising phases in response to contralateral sounds, independent of the neuron's preferred location as determined by response amplitude, which is consistent with our finding that the latencies of both excitatory and inhibitory inputs to A1 neurons are shorter for contralateral sounds, and that excitation (but not inhibition) exhibits steeper rising phases in response to contralateral sounds. We emphasize that Chadderton and colleagues' findings are also consistent with other patterns of synaptic input, such as earlier arrival of excitation for contralateral sounds, but no change for inhibition, or steeper rising phases for both excitatory and inhibitory conductance changes, for example.

Membrane potential recordings are more informative than spiking records alone, but in the absence of other manipulations, they cannot rule out the possibility that decreases in the membrane potential are due to decreases in excitation rather than increases in inhibition. Accordingly, Ojima and Murakami (Ojima & Murakami, 2002) employed two manipulations — varying the Cl^- concentration in the recording pipette and injecting constant depolarizing or hyperpolarizing current — to confirm that the hyperpolarization they observed was in fact due to synaptic inhibition to the recorded neuron. However, they did not attempt to reconstruct timecourses or even temporal averages of inhibitory or excitatory synaptic conductances and they only presented six cells for their binaural analysis.

Imaging studies in human cortex have also found a contralateral preference for monaural stimulation (Woldorff et al., 1999; Petkov et al., 2004; Krumbholz et al., 2005), but no preference for more realistic binaural stimulation (Woldorff et al., 1999; Brunetti et al., 2005; Krumbholz et al., 2005; Zimmer and Macaluso, 2005; Zimmer et al., 2006). This apparent discrepancy with animal studies likely reflects the heterogeneity of nearby neurons in A1 and throughout AC (Werner-Reiss and Groh, 2008), pointing to the need for continued single-unit studies. There have been reports of bands (Imig and Adrian, 1977; Middlebrooks et al., 1980) and clusters (Reale and Kettner, 1986; Kelly and Sally, 1988; Clarey et al., 1994; Kelly and Judge, 1994; Shen et al., 1997; Razak and Fuzessery, 2000; Rutkowski et al., 2000a) of direction or binaurally selective units in A1, but both spatially-sensitive and spatially-invariant units have been observed throughout the full extent of A1.

Like spike count, spike timing can convey information about sound source location (Brugge et al., 1996; Mickey and Middlebrooks, 2003; Reale et al., 2003; Mrsic-Flogel et al., 2005; Nelken et al., 2005) and offer clues about the underlying mechanisms (Kitzes et al., 1980), but any observed pattern of spiking responses could result from multiple candidate mechanisms.

Fortunately, *in vivo* whole-cell recording in *voltage-clamp* mode does allow for the decomposition of synaptic input into excitatory and inhibitory components. However, all currently available data of this type from AC was obtained during contralateral stimulation alone, whether in natural free-field conditions (Wehr and Zador, 2003; Zhang et al., 2003; Tan et al., 2004; Wehr and Zador, 2005; Liu et al., 2007; Tan et al., 2007; Scholl et al., 2008; Scholl and Wehr, 2008), with the ipsilateral ear plugged (Wu et al., 2006; Wu et al., 2008), or using monaural dichotic stimulation to the contralateral ear (Froemke et al., 2007) (or not reported (Las et al., 2005)). To our knowledge, there are no published reports of measured excitatory and inhibitory conductances in response to acoustic stimulation originating from systematically varied sound source locations, though Wehr and colleagues have reported preliminary findings (M. Kyweriga, W. N. Wolfe, C. C. Cahill, M. Wehr, Synaptic mechanisms of binaural interactions in rat primary auditory cortex, Society for Neuroscience Abstracts, 2010).

We did not find any clear trends between the patterns of synaptic drive and laminar position of recorded neurons, as inferred from electrode travel from the cortical surface to the recording sites (data not shown). Due to brain dimpling, electrode travel is only a crude measure of laminar position, but patch clamp recording methods offer the possibility of filling cells with biocytin or other agents, allowing for histological

reconstruction of labeled neurons. In future work, it will be interesting to correlate spatial sensitivity of excitatory and inhibitory input to individual neurons with laminar position and cell type.

References

Anderson JS, Carandini M, Ferster D (2000) Orientation tuning of input conductance, excitation, and inhibition in cat primary visual cortex. J Neurophysiol 84:909-926.

Azouz R, Gray CM, Nowak LG, McCormick DA (1997) Physiological properties of inhibitory interneurons in cat striate cortex. Cereb Cortex 7:534-545.

Bizley JK, Walker KM, Silverman BW, King AJ, Schnupp JW (2009) Interdependent encoding of pitch, timbre, and spatial location in auditory cortex. J Neurosci 29:2064-2075.

Borg-Graham LJ, Monier C, Fregnac Y (1998) Visual input evokes transient and strong shunting inhibition in visual cortical neurons. Nature 393:369-373.

Bringuier V, Chavane F, Glaeser L, Fregnac Y (1999) Horizontal propagation of visual activity in the synaptic integration field of area 17 neurons. Science 283:695-699.

Brown TH, Zador AM, Mainen ZF, Claiborne BJ (1992) Hebbian computations in hippocampal dendrites and spines. In: Single neuron computation. (McKenna TM, Davis J, et al., eds), pp 81-116. San Diego, CA, US: Academic Press, Inc.

Brugge JF, Reale RA, Hind JE (1996) The structure of spatial receptive fields of neurons in primary auditory cortex of the cat. J Neurosci 16:4420-4437.

Brugge JF, Dubrovsky NA, Aitkin LM, Anderson DJ (1969) Sensitivity of single neurons in auditory cortex of cat to binaural tonal stimulation; effects of varying interaural time and intensity. J Neurophysiol 32:1005-1024.

Brugge JF, Reale RA, Hind JE, Chan JC, Musicant AD, Poon PW (1994) Simulation of free-field sound sources and its application to studies of cortical mechanisms of sound localization in the cat. Hear Res 73:67-84.

Brunetti M, Belardinelli P, Caulo M, Del Gratta C, Della Penna S, Ferretti A, Lucci G, Moretti A, Pizzella V, Tartaro A, Torquati K, Olivetti Belardinelli M, Romani GL (2005) Human brain activation during passive listening to sounds from different locations: an fMRI and MEG study. Hum Brain Mapp 26:251-261.

Bureau I, Shepherd GM, Svoboda K (2004) Precise development of functional and anatomical columns in the neocortex. Neuron 42:789-801.

Calford MB, Semple MN (1995) Monaural inhibition in cat auditory cortex. J Neurophysiol 73:1876-1891.

Campbell RA, Schnupp JW, Shial A, King AJ (2006) Binaural-level functions in ferret auditory cortex: evidence for a continuous distribution of response properties. J Neurophysiol 95:3742-3755.

Cang J, Isaacson JS (2003) In vivo whole-cell recording of odor-evoked synaptic transmission in the rat olfactory bulb. J Neurosci 23:4108-4116.

Chadderton P, Agapiou JP, McAlpine D, Margrie TW (2009) The synaptic representation of sound source location in auditory cortex. J Neurosci 29:14127-14135.

Claiborne BJ, Zador AM, Mainen ZF, Brown TH (1992) Computational models of hippocampal neurons. In: Single neuron computation. (McKenna TM, Davis J, et al., eds), pp 61-80. San Diego, CA, US: Academic Press, Inc.

Clarey JC, Barone P, Imig TJ (1994) Functional organization of sound direction and sound pressure level in primary auditory cortex of the cat. J Neurophysiol 72:2383-2405.

Clarey JC, Barone P, Irons WA, Samson FK, Imig TJ (1995) Comparison of noise and tone azimuth tuning of neurons in cat primary auditory cortex and medical geniculate body. J Neurophysiol 74:961-980.

Covey E, Kauer JA, Casseday JH (1996) Whole-cell patch-clamp recording reveals subthreshold sound-evoked postsynaptic currents in the inferior colliculus of awake bats. J Neurosci 16:3009-3018.

DeWeese MR (2007) Whole-cell recording in vivo. Curr Protoc Neurosci Chapter 6:Unit 6 22.

DeWeese MR, Zador AM (2004) Shared and private variability in the auditory cortex. J Neurophysiol 92:1840-1855.

DeWeese MR, Zador AM (2006) Non-Gaussian membrane potential dynamics imply sparse, synchronous activity in auditory cortex. J Neurosci 26:12206-12218.

DeWeese MR, Wehr M, Zador AM (2003) Binary spiking in auditory cortex. J Neurosci 23:7940-7949.

Dorrn AL, Yuan K, Barker AJ, Schreiner CE, Froemke RC (2010) Developmental sensory experience balances cortical excitation and inhibition. Nature 465:932-936.

Ferster D, Jagadeesh B (1992) EPSP-IPSP interactions in cat visual cortex studied with in vivo whole- cell patch recording. J Neurosci 12:1262-1274.

Freeman TC, Durand S, Kiper DC, Carandini M (2002) Suppression without inhibition in visual cortex. Neuron 35:759-771.

Froemke RC, Merzenich MM, Schreiner CE (2007) A synaptic memory trace for cortical receptive field plasticity. Nature 450:425-429.

Gao L, Meng X, Ye C, Zhang H, Liu C, Dan Y, Poo MM, He J, Zhang X (2009) Entrainment of slow oscillations of auditory thalamic neurons by repetitive sound stimuli. J Neurosci 29:6013-6021.

Goldberg JM, Brown PB (1969) Response of binaural neurons of dog superior olivary complex to dichotic tonal stimuli: some physiological mechanisms of sound localization. J Neurophysiol 32:613-636.

Gray CM, McCormick DA (1996) Chattering cells: superficial pyramidal neurons contributing to the generation of synchronous oscillations in the visual cortex. Science 274:109-113.

Hall JL, 2nd, Goldstein MH, Jr. (1968) Representation of binaural stimuli by single units in primary auditory cortex of unanesthetized cats. J Acoust Soc Am 43:456-461.

Heffner H, Masterton B (1975) Contribution of auditory cortex to sound localization in the monkey (Macaca mulatta). J Neurophysiol 38:1340-1358.

Hirsch JA, Alonso JM, Reid RC (1995) Visually evoked calcium action potentials in cat striate cortex. Nature 378:612-616.

Hirsch JA, Alonso JM, Reid RC, Martinez LM (1998) Synaptic integration in striate cortical simple cells. J Neurosci 18:9517-9528.

Houweling AR, Brecht M (2008) Behavioural report of single neuron stimulation in somatosensory cortex. Nature 451:65-68.

Hu B, Senatorov V, Mooney D (1994) Lemniscal and non-lemniscal synaptic transmission in rat auditory thalamus. J Physiol 479:217-231.

Imig TJ, Adrian HO (1977) Binaural columns in the primary field (A1) of cat auditory cortex. Brain Res 138:241-257.

Imig TJ, Irons WA, Samson FR (1990) Single-unit selectivity to azimuthal direction and sound pressure level of noise bursts in cat high-frequency primary auditory cortex. J Neurophysiol 63:1448-1466.

Irvine DR, Rajan R, Aitkin LM (1996) Sensitivity to interaural intensity differences of neurons in primary auditory cortex of the cat. I. types of sensitivity and effects of variations in sound pressure level. J Neurophysiol 75:75-96.

Jenkins WM, Masterton RB (1982) Sound localization: effects of unilateral lesions in central auditory system. J Neurophysiol 47:987-1016.

Jenkins WM, Merzenich MM (1984) Role of cat primary auditory cortex for sound-localization behavior. J Neurophysiol 52:819-847.

Kavanagh GL, Kelly JB (1987) Contribution of auditory cortex to sound localization by the ferret (Mustela putorius). J Neurophysiol 57:1746-1766.

Kelly JB (1980) Effects of auditory cortical lesions on sound localization by the rat. J Neurophysiol 44:1161-1174.

Kelly JB, Sally SL (1988) Organization of auditory cortex in the albino rat: binaural response properties. J Neurophysiol 59:1756-1769.

Kelly JB, Judge PW (1994) Binaural organization of primary auditory cortex in the ferret (Mustela putorius). J Neurophysiol 71:904-913.

King AJ, Schnupp JW, Doubell TP (2001) The shape of ears to come: dynamic coding of auditory space. Trends Cogn Sci 5:261-270.

King AJ, Bajo VM, Bizley JK, Campbell RA, Nodal FR, Schulz AL, Schnupp JW (2007) Physiological and behavioral studies of spatial coding in the auditory cortex. Hear Res 229:106-115.

Kitzes LM, Wrege KS, Cassady JM (1980) Patterns of responses of cortical cells to binaural stimulation. J Comp Neurol 192:455-472.

Klingon GH, Bontecou DC (1966) Localization in auditory space. Neurology 16:879-886.

Koch C, Poggio T, Torre V (1982) Retinal ganglion cells: a functional interpretation of dendritic morphology. Philos Trans R Soc Lond B Biol Sci 298:227-263.

Krumbholz K, Schonwiesner M, von Cramon DY, Rubsamen R, Shah NJ, Zilles K, Fink GR (2005) Representation of interaural temporal information from left and right auditory space in the human planum temporale and inferior parietal lobe. Cereb Cortex 15:317-324.

Las L, Stern EA, Nelken I (2005) Representation of tone in fluctuating maskers in the ascending auditory system. J Neurosci 25:1503-1513.

Liu BH, Wu GK, Arbuckle R, Tao HW, Zhang LI (2007) Defining cortical frequency tuning with recurrent excitatory circuitry. Nat Neurosci 10:1594-1600.

Mainen ZF, Carnevale NT, Zador AM, Claiborne BJ, Brown TH (1996) Electrotonic architecture of hippocampal CA1 pyramidal neurons based on three-dimensional reconstructions. J Neurophysiol 76:1904-1923.

Manns ID, Sakmann B, Brecht M (2004) Sub- and suprathreshold receptive field properties of pyramidal neurones in layers 5A and 5B of rat somatosensory barrel cortex. J Physiol 556:601-622.

Margrie TW, Brecht M, Sakmann B (2002) In vivo, low-resistance, whole-cell recordings from neurons in the anaesthetized and awake mammalian brain. Pfluegers Archiv European Journal of Physiology 444:491-498.

McAlpine D (2005) Creating a sense of auditory space. J Physiol 566:21-28.

Meliza CD, Dan Y (2006) Receptive-field modification in rat visual cortex induced by paired visual stimulation and single-cell spiking. Neuron 49:183-189.

Metherate R, Ashe JH (1993) Ionic flux contributions to neocortical slow waves and nucleus basalis-mediated activation: whole-cell recordings in vivo. J Neurosci 13:5312-5323.

Mickey BJ, Middlebrooks JC (2003) Representation of auditory space by cortical neurons in awake cats. J Neurosci 23:8649-8663.

Middlebrooks JC, Pettigrew JD (1981) Functional classes of neurons in primary auditory cortex of the cat distinguished by sensitivity to sound location. J Neurosci 1:107-120.

Middlebrooks JC, Dykes RW, Merzenich MM (1980) Binaural response-specific bands in primary auditory cortex (AI) of the cat: topographical organization orthogonal to isofrequency contours. Brain Res 181:31-48.

Moore CI, Nelson SB (1998) Spatio-temporal subthreshold receptive fields in the vibrissa representation of rat primary somatosensory cortex. J Neurophysiol 80:2882-2892.

Mrsic-Flogel TD, King AJ, Schnupp JW (2005) Encoding of virtual acoustic space stimuli by neurons in ferret primary auditory cortex. J Neurophysiol 93:3489-3503.

Mrsic-Flogel TD, King AJ, Jenison RL, Schnupp JW (2001) Listening through different ears alters spatial response fields in ferret primary auditory cortex. J Neurophysiol 86:1043-1046.

Nelken I, Chechik G, Mrsic-Flogel TD, King AJ, Schnupp JW (2005) Encoding stimulus information by spike numbers and mean response time in primary auditory cortex. J Comput Neurosci 19:199-221.

Nelson S, Toth L, Sheth B, Sur M (1994) Orientation selectivity of cortical neurons during intracellular blockade of inhibition. Science 265:774-777.

Nodal FR, Kacelnik O, Bajo VM, Bizley JK, Moore DR, King AJ (2010) Lesions of the auditory cortex impair azimuthal sound localization and its recalibration in ferrets. J Neurophysiol 103:1209-1225.

Ojima H, Murakami K (2002) Intracellular characterization of suppressive responses in supragranular pyramidal neurons of cat primary auditory cortex in vivo. Cereb Cortex 12:1079-1091.

Okun M, Lampl I (2008) Instantaneous correlation of excitation and inhibition during ongoing and sensory-evoked activities. Nat Neurosci 11:535-537.

Petkov CI, Kang X, Alho K, Bertrand O, Yund EW, Woods DL (2004) Attentional modulation of human auditory cortex. Nat Neurosci 7:658-663.

Phillips DP, Cynader MS (1985) Some neural mechanisms in the cat's auditory cortex underlying sensitivity to combined tone and wide-spectrum noise stimuli. Hear Res 18:87-102.

Priebe NJ (2008) The relationship between subthreshold and suprathreshold ocular dominance in cat primary visual cortex. J Neurosci 28:8553-8559.

Rajan R, Aitkin LM, Irvine DR, McKay J (1990) Azimuthal sensitivity of neurons in primary auditory cortex of cats. I. Types of sensitivity and the effects of variations in stimulus parameters. J Neurophysiol 64:872-887.

Razak KA, Fuzessery ZM (2000) A systematic representation of interaural intensity differences in the auditory cortex of the pallid bat. Neuroreport 11:2919-2924.

Reale RA, Kettner RE (1986) Topography of binaural organization in primary auditory cortex of the cat: effects of changing interaural intensity. J Neurophysiol 56:663-682.

Reale RA, Jenison RL, Brugge JF (2003) Directional sensitivity of neurons in the primary auditory (AI) cortex: effects of sound-source intensity level. J Neurophysiol 89:1024-1038.

Reyes A (2001) Influence of dendritic conductances on the input-output properties of neurons. Annu Rev Neurosci 24:653-675.

Rutkowski RG, Wallace MN, Shackleton TM, Palmer AR (2000a) Organisation of binaural interactions in the primary and dorsocaudal fields of the guinea pig auditory cortex. Hear Res 145:177-189.

Rutkowski RG, Wallace MN, Shackleton TM, Palmer AR (2000b) Organisation of binaural interactions in the primary and dorsocaudal fields of the guinea pig auditory cortex. Hear Res 145:177-189.

Sanchez-Longo LP, Forster FM (1958) Clinical significance of impairment of sound localization. Neurology 8:119-125.

Sanes DH, Malone BJ, Semple MN (1998) Role of synaptic inhibition in processing of dynamic binaural level stimuli. J Neurosci 18:794-803.

Schnupp JW, Mrsic-Flogel TD, King AJ (2001) Linear processing of spatial cues in primary auditory cortex. Nature 414:200-204.

Schnupp JW, Booth J, King AJ (2003) Modeling individual differences in ferret external ear transfer functions. J Acoust Soc Am 113:2021-2030.

Scholl B, Wehr M (2008) Disruption of balanced cortical excitation and inhibition by acoustic trauma. J Neurophysiol 100:646-656.

Scholl B, Gao X, Wehr M (2008) Level dependence of contextual modulation in auditory cortex. J Neurophysiol 99:1616-1627.

Shen JX, Chen QC, Jen PH (1997) Binaural and frequency representation in the primary auditory cortex of the big brown bat, Eptesicus fuscus. J Comp Physiol [A] 181:591-597.

Spruston N, Jaffe DB, Williams SH, Johnston D (1993) Voltage- and space-clamp errors associated with the measurement of electrotonically remote synaptic events. J Neurophysiol 70:781-802.

Stecker GC, Harrington IA, Middlebrooks JC (2005) Location coding by opponent neural populations in the auditory cortex. PLoS Biol 3:e78.

Suga N (1971) Responses of inferior collicular neurones of bats to tone bursts with different rise times. J Physiol 217:159-177.

Sun W, Dan Y (2009) Layer-specific network oscillation and spatiotemporal receptive field in the visual cortex. Proc Natl Acad Sci U S A 106:17986-17991.

Talwar SK, Musial PG, Gerstein GL (2001) Role of Mammalian Auditory Cortex in the Perception of Elementary Sound Properties. J Neurophysiol 85:2350-2358.

Tan AY, Zhang LI, Merzenich MM, Schreiner CE (2004) Tone-evoked excitatory and inhibitory synaptic conductances of primary auditory cortex neurons. J Neurophysiol 92:630-643.

Tan AY, Atencio CA, Polley DB, Merzenich MM, Schreiner CE (2007) Unbalanced synaptic inhibition can create intensity-tuned auditory cortex neurons. Neuroscience 146:449-462.

Voigt HF, Young ED (1980) Evidence of inhibitory interactions between neurons in dorsal cochlear nucleus. J Neurophysiol 44:76-96.

Wehr M, Zador AM (2003) Balanced inhibition underlies tuning and sharpens spike timing in auditory cortex. Nature 426:442-446.

Wehr M, Zador AM (2005) Synaptic mechanisms of forward suppression in rat auditory cortex. Neuron 47:437-445.

Werner-Reiss U, Groh JM (2008) A rate code for sound azimuth in monkey auditory cortex: implications for human neuroimaging studies. J Neurosci 28:3747-3758.

Williams SR, Mitchell SJ (2008) Direct measurement of somatic voltage clamp errors in central neurons. Nat Neurosci 11:790-798.

Woldorff MG, Tempelmann C, Fell J, Tegeler C, Gaschler-Markefski B, Hinrichs H, Heinz HJ, Scheich H (1999) Lateralized auditory spatial perception and the contralaterality of cortical processing as studied with functional magnetic resonance imaging and magnetoencephalography. Hum Brain Mapp 7:49-66.

Wu GK, Li P, Tao HW, Zhang LI (2006) Nonmonotonic synaptic excitation and imbalanced inhibition underlying cortical intensity tuning. Neuron 52:705-715.

Wu GK, Arbuckle R, Liu BH, Tao HW, Zhang LI (2008) Lateral sharpening of cortical frequency tuning by approximately balanced inhibition. Neuron 58:132-143.

Zador AM, Agmon-Snir H, Segev I (1995) The morphoelectrotonic transform: a graphical approach to dendritic function. J Neurosci 15:1669-1682.

Zhang J, Nakamoto KT, Kitzes LM (2004) Binaural interaction revisited in the cat primary auditory cortex. J Neurophysiol 91:101-117.

Zhang LI, Tan AY, Schreiner CE, Merzenich MM (2003) Topography and synaptic shaping of direction selectivity in primary auditory cortex. Nature 424:201-205.

Zhu JJ, Connors BW (1999a) Intrinsic firing patterns and whisker-evoked synaptic responses of neurons in the rat barrel cortex. J Neurophysiol 81:1171-1183.

Zhu JJ, Connors BW (1999b) Intrinsic firing patterns and whisker-evoked synaptic responses of neurons in the rat barrel cortex. J Neurophysiol 81:1171-1183.

Zhu Y, Zhu JJ (2004) Rapid arrival and integration of ascending sensory information in layer 1 nonpyramidal neurons and tuft dendrites of layer 5 pyramidal neurons of the neocortex. J Neurosci 24:1272-1279.

Zimmer U, Macaluso E (2005) High binaural coherence determines successful sound localization and increased activity in posterior auditory areas. Neuron 47:893-905.

Zimmer U, Lewald J, Erb M, Karnath HO (2006) Processing of auditory spatial cues in human cortex: an fMRI study. Neuropsychologia 44:454-461.

Figure 1: Several candidate synaptic mechanisms could underlie spatial sensitivity in A1. ***A*** Cartoons of spike rasters (*top*) and peri-stimulus time histograms (*bottom*) elicited from the same hypothetical neuron in response to sounds (*purple and blue bars*) originating from sources located ipsilateral (*left*) or contralateral (*right*) to the recorded neuron; this model neuron prefers contralateral stimulation, as do the majority of A1 neurons. The reduced responsiveness to ipsilateral sounds compared with that of contralateral sounds might be due to: ***B*** a reduction in the peak excitatory synaptic conductance (g_e; *green curve*), but no change in the inhibitory conductance (g_i ; *red curve*), in the recorded neuron; ***C*** an increase in the peak value of the inhibition alone; ***D*** a proportional decrease in both excitation and inhibition; ***E*** a change in the relative timing of the excitatory and inhibitory drive; or some combination of these or other effects.

Figure 2: Measuring the timecourses of auditory-evoked excitatory and inhibitory synaptic conductances in A1 using *in vivo* whole-cell patch clamp recording in voltage clamp mode. ***A*** Three current traces measured while holding the neuron's membrane potential at different voltages (5 mV, *blue*; -80 mV, *purple*; -110 mV, *violet*; values adjusted for the -10 mV junction potential we calculated for our Cs-gluconate-based internal solution). Each curve is an average of 250 trials in response to 100 msec white noise bursts presented from a speaker located contralateral to the recorded neuron. Action potentials were blocked intracellularly with the sodium channel blocker QX-314. ***B*** Instantaneous synaptic-voltage (I-V) curve corresponding to the time of the peak in the total conductance. ***C*** Total synaptic conductance (*black*) and its decomposition into excitation (*green*) and inhibition (*red*) (see Materials and Methods).

Figure 3: Comparison of auditory-evoked synaptic input to an A1 neuron resulting from different sound source locations. Timecourses of the excitatory (*green*) and inhibitory (*red*) synaptic conductances of an A1 neuron responding to the onsets (*blue and purple hash marks the two color are not distinguishable)* of 100 msec white noise bursts at seven sound intensities from a speaker located ipsilateral (*left panels*) or contralateral (*right panels*) to the recorded neuron. This neuron displays several effects evident across the recorded population: For each sound intensity tested, sounds originating contralateral to the recorded neuron typically induced greater peak excitatory and inhibitory responses compared with ipsilateral sounds, broadly consistent with Fig. 1D. Contralateral sounds tended to induce earlier latencies for both excitation and inhibition compared to ipsilateral sounds. Excitation tended to precede inhibition for both contralateral and ipsilateral sounds. The initial rising phase of the inhibitory conductance tended to be steeper than that of the excitatory conductance timecourse, which was true for both ipsilateral and contralateral sounds across the population. Note that this neuron also presents some deviations from this simple description, such as the unbalanced recruitment of excitation and inhibition with increasing intensity for contralateral sounds, and the surprisingly small change in the timecourse or amplitude of either excitation or inhibition in response to ipsilateral stimulation over the full range of sound intensity we tested. As with all neurons in this study, the recording site was in the left hemisphere, so the right speaker was contralateral to the neuron.

Figure 4: Across the population, both synaptic excitation and inhibition to individual A1 neurons show the same contralateral preference as spiking responses in A1 and in the auditory thalamus (ventral division of the medial geniculate body; MGBv). ***A*** Across the

population (N = 30 cells; 7 sound intensity levels), peak excitatory conductances (*green, upward pointing triangles*) were higher on average for contralateral sounds compared to ipsilateral sounds ($p = 2.1\times10^{-8}$; all p values reported here are for the two-tailed Wilcoxon signed rank test). This was also the case for peak inhibitory conductances (*red, downward pointing triangles*; $p = 1.7\times10^{-12}$). ***B*** This contralateral preference was evident for responses restricted to only the greatest sound intensity level we tested (excitation: $p = 2.3\times10^{-4}$; inhibition: $p = 0.0098$). ***C*** Both excitatory and inhibitory synaptic drive tended to arrive sooner in response to sounds from contralateral sources compared to ipsilateral sources (excitation: $p = 5.2\times10^{-4}$; inhibition: $p = 1.1\times10^{-6}$), as one might expect given the greater peak values in response to contralateral sounds. ***D*** This was also true for responses restricted to the loudest sound levels tested (excitation: $p = 0.0010$; inhibition: $p = 9.3\times10^{-5}$).

Figure 5: Excitation and inhibition are approximately balanced for individual A1 neurons, so that the ratio of peak excitatory and inhibitory conductances is roughly constant across sound levels for specific sound source locations. ***A*** An example neuron exhibiting a strong correlation between peak inhibitory and excitatory conductances across sound intensity levels for a contralateral sound source (*purple, rightward pointing triangles*; $r = 0.81$, Pearson product-moment correlation coefficient), as well as for an ipsilateral sound source (*blue, leftward pointing triangles*; $r = 0.87$). For this neuron, the ratio of the peak values of inhibitory to excitatory conductance was approximately 2.5 for contralateral sounds, and 1.1 for ipsilateral sounds. ***B*** A scatterplot of pairs of correlation coefficients (as in panel *A*) across the population shows that peak excitatory and inhibitory conductances of many neurons are strongly correlated, with population

averaged correlations of r = 0.74 ± 0.05 and 0.54 ± 0.09 (mean ± SEM; *red square*) for contralateral and ipsilateral sources, respectively. ***C*** A scatterplot of peak excitatory and inhibitory conductances including all neurons and all sound intensity levels. ***D*** The fraction of excitatory conductance — $g_{ep}/(g_{ep} + g_{ip})$, where g_{ep} (g_{ip}) is the peak excitatory (inhibitory) conductance — is peaked near the intermediate value of 0.35 for both contralateral and ipsilateral sources, which is also close to the mean values for each distribution (contralateral: μ ± SEM = 0.39 ± 0.01; ipsilateral: μ ± SEM = 0.44 ± 0.01). Across the population, few responses are dominated by either excitation or inhibition alone. ***E*** For both contralateral and ipsilateral sound sources, excitation tends to arrive slightly sooner than inhibition (contralateral: $t_i - t_e$ = 0.73 msec, p = 0.042; ipsilateral: $t_i - t_e$ = 1.3 msec, p = 0.0035; two-tailed Wilcoxon signed rank test), as previously reported for synaptic responses to contralateral sounds (Wehr and Zador, 2003; Zhang et al., 2003; Tan et al., 2004; Wu et al., 2006; Wu et al., 2008). Histogram and analysis included only those responses for which peak excitatory and peak inhibitory conductances summed to 1 nS or more.

Figure 6: The slope of the initial rising phase of excitatory conductance changes was greater in response to contralateral sound sources compared with ipsilateral sounds, and inhibitory conductances had steeper rising phases than excitatory conductances for both ipsilateral and contralateral sound sources. ***A*** A scatterplot of the slope of the rising phase of the excitatory conductance changes (*green, upward pointing triangles*) demonstrates that contralateral sounds elicited steeper rising phases than ipsilateral sounds ($p = 4.5\times10^{-4}$; all p values refer to the two-tailed Wilcoxon signed rank test) for the highest sound intensity we tested. Inhibitory responses, however, did not show a

statistically significant difference in slope between ipsilateral and contralateral sounds (p = 0.27). ***B*** The initial rising phase of the inhibitory synaptic conductance was consistently steeper than that of the excitatory conductance for both contralateral ($p = 1.5\times10^{-5}$) and ipsilateral ($p = 1.2\times10^{-5}$) sound sources.

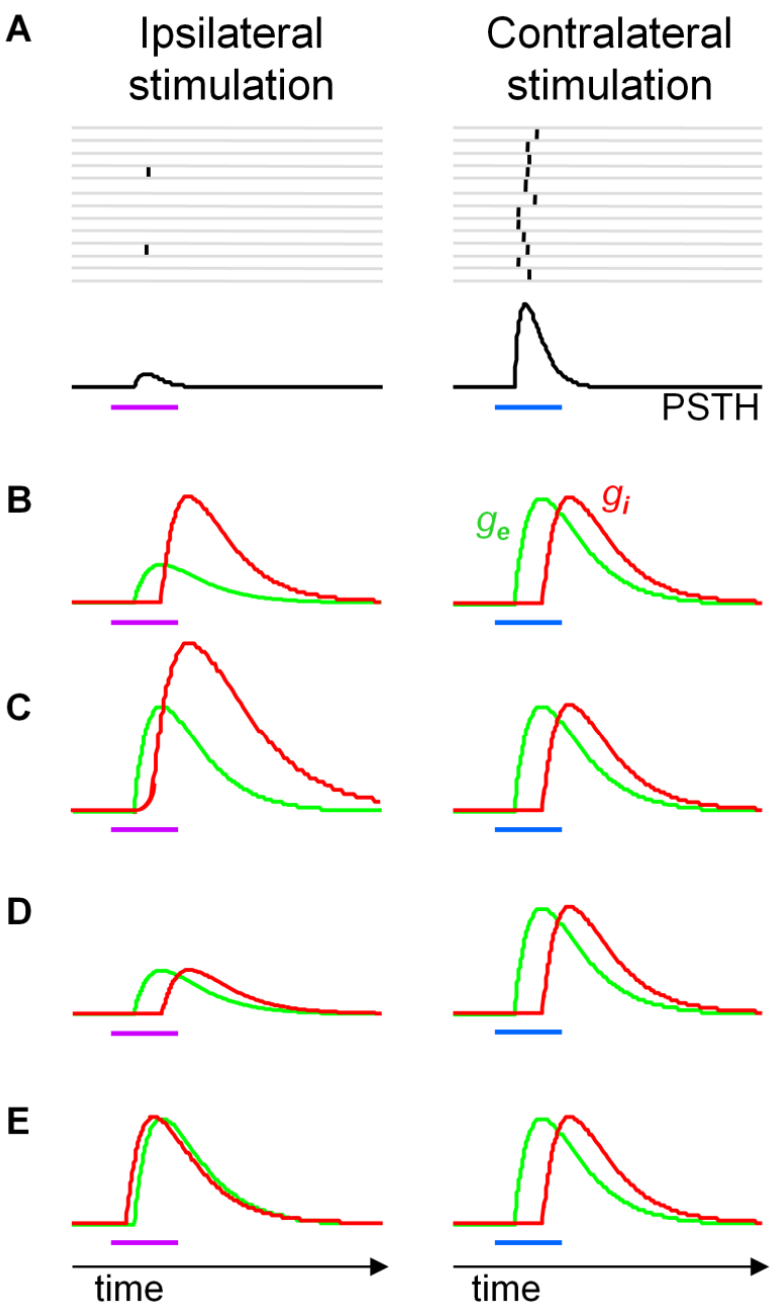

DeWeese Figure 1

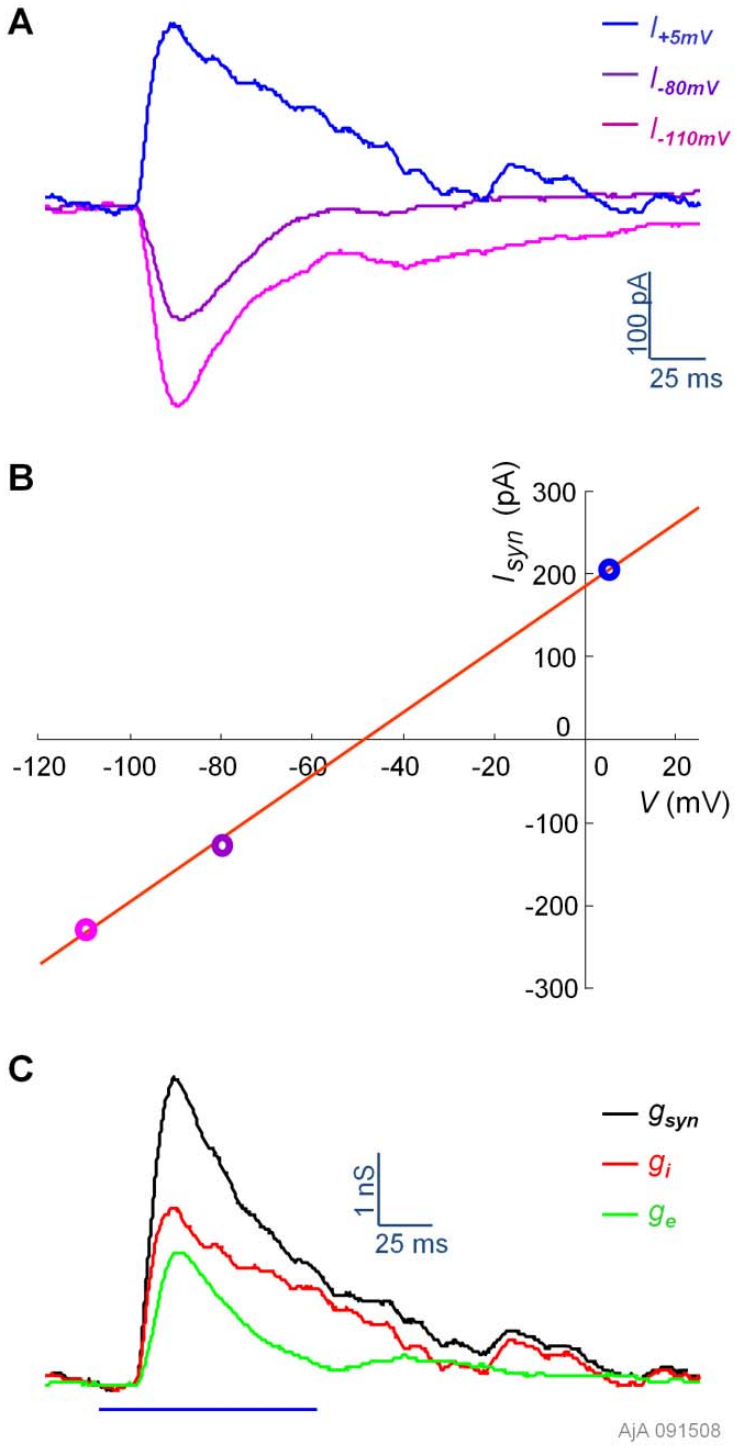

DeWeese Figure 2

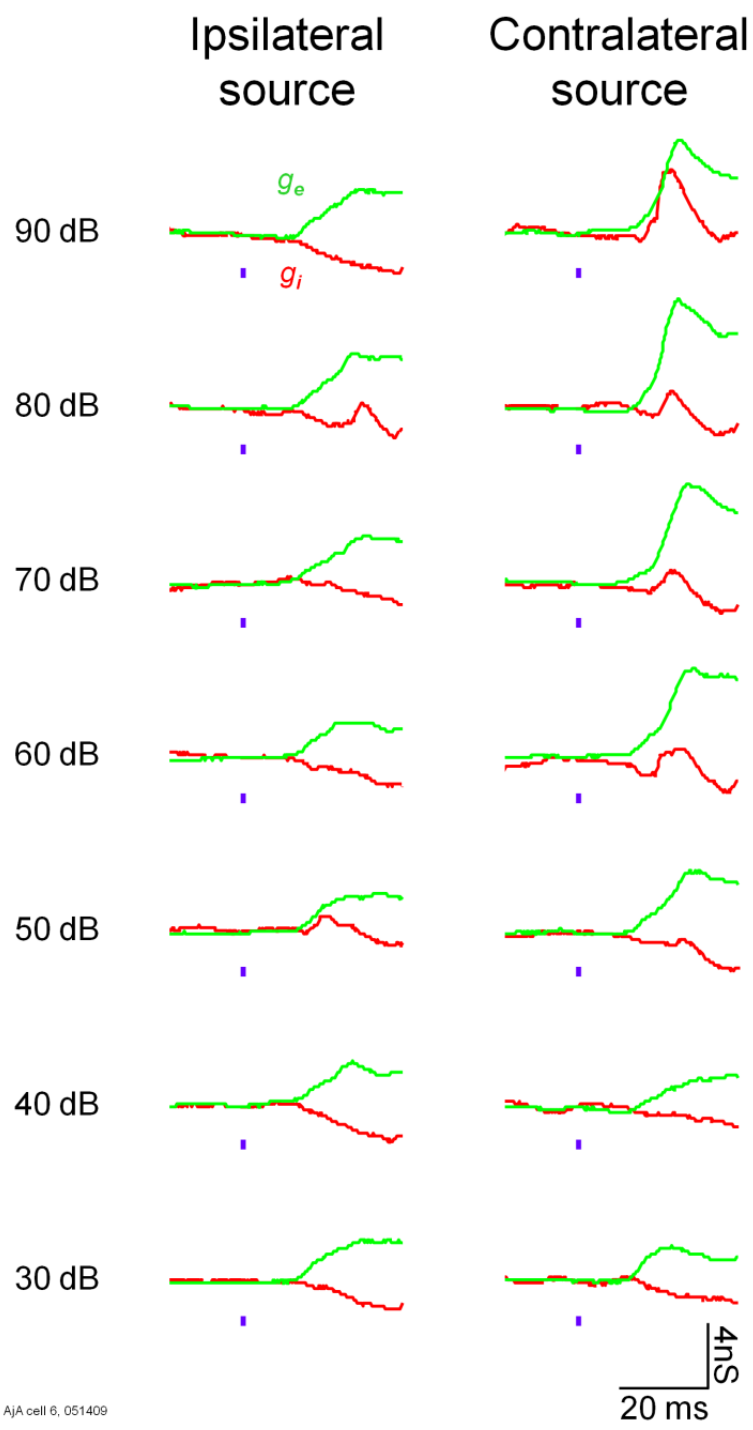

DeWeese Figure 3

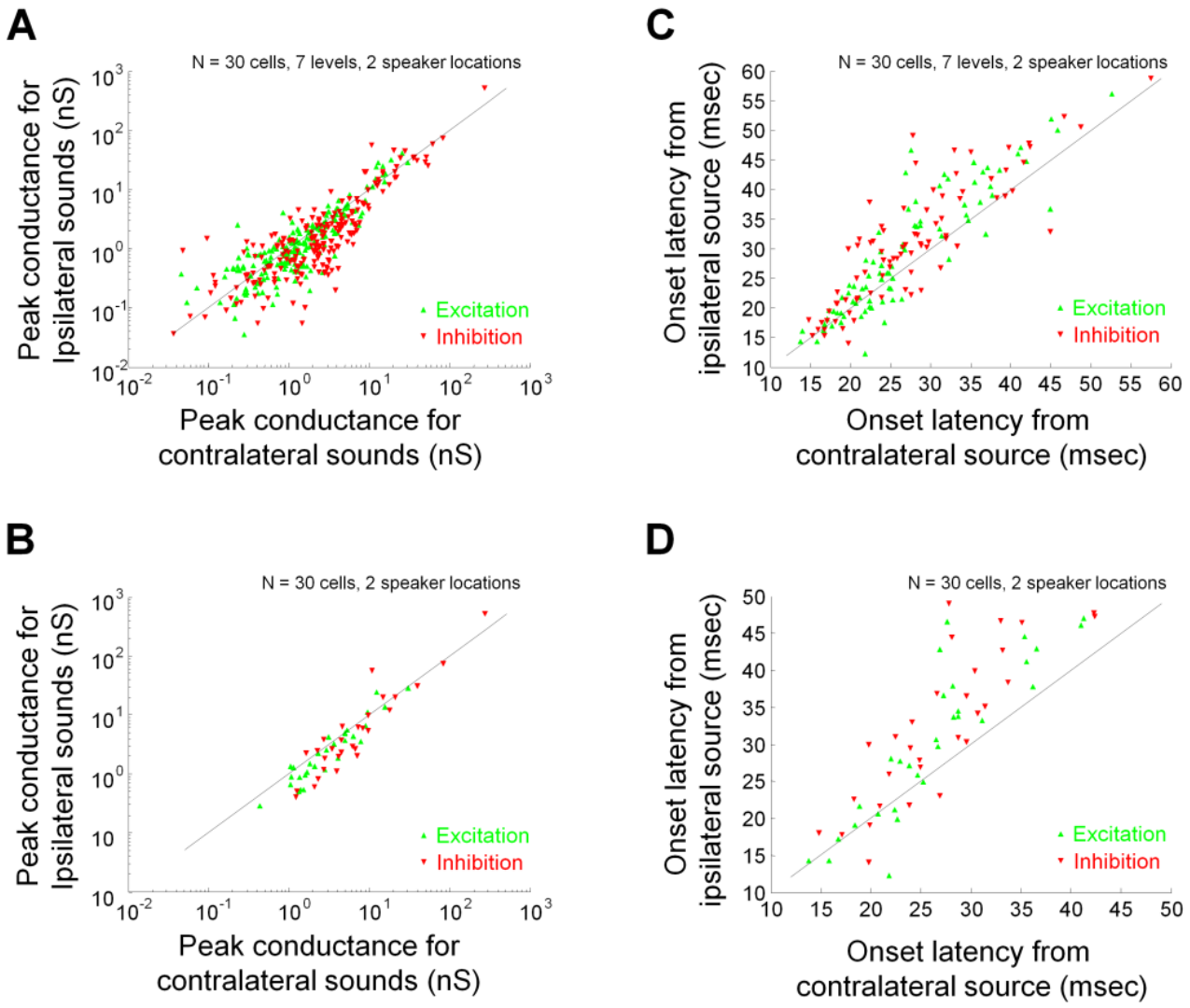

DeWeese Figure 4

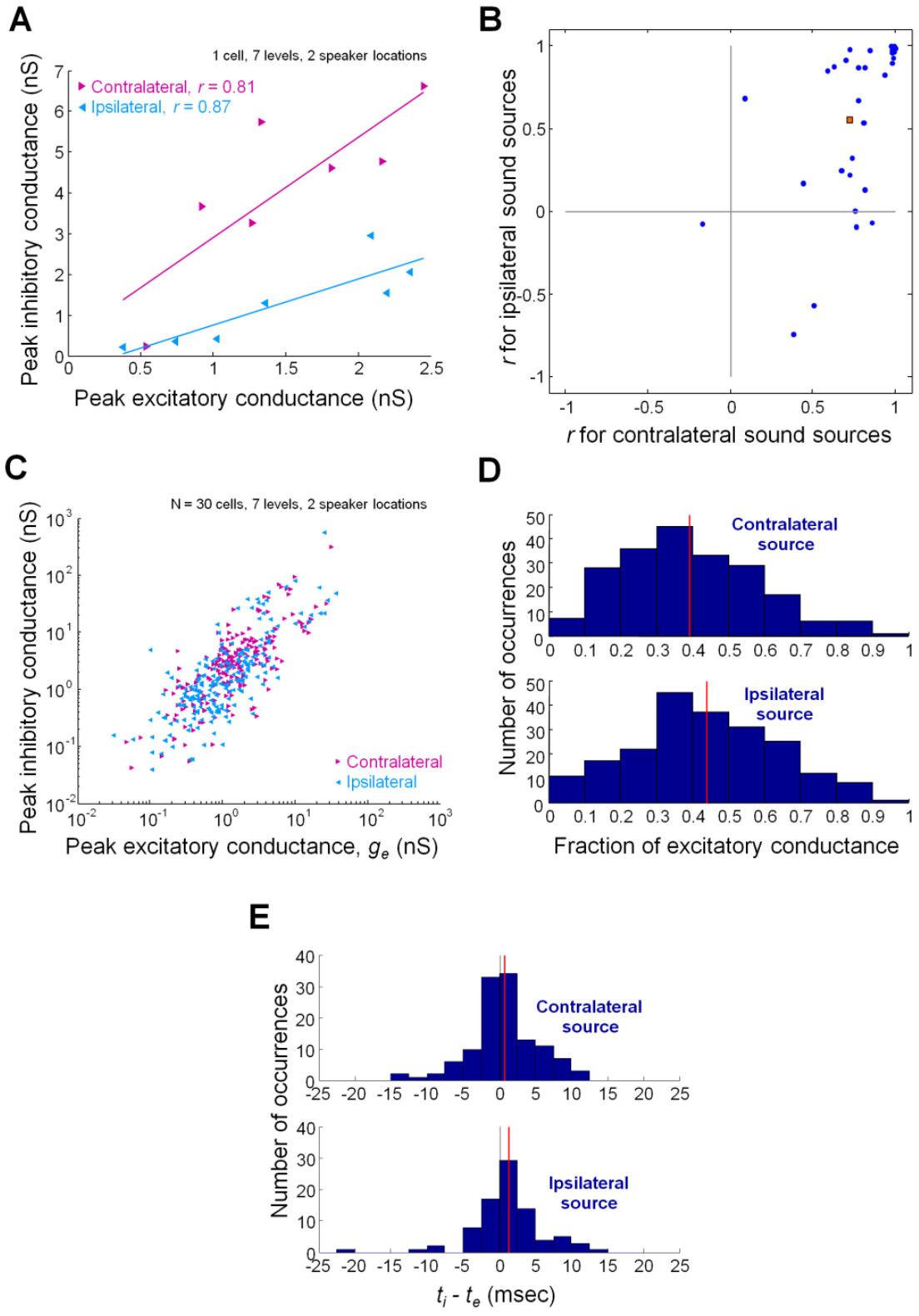

DeWeese Figure 5

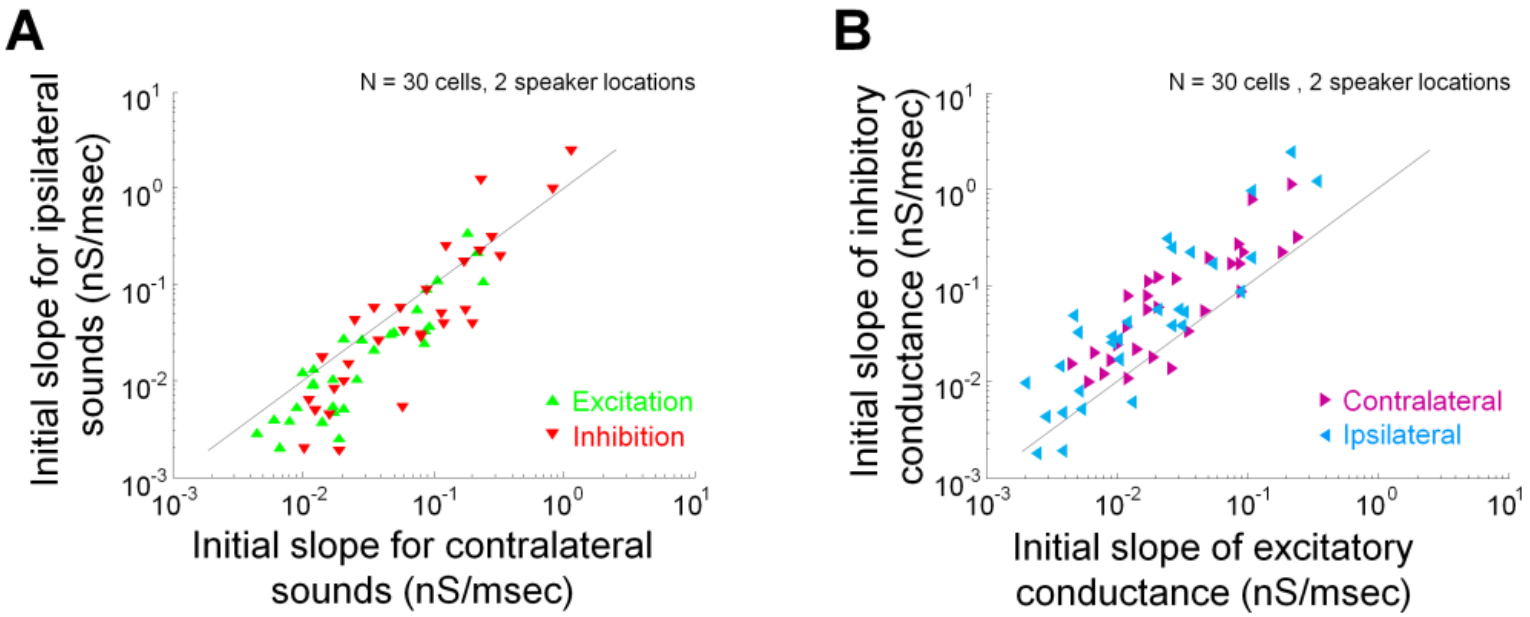

DeWeese Figure 6